



Are D2D and RIS in the same league? Cooperative RSSI-based localization model and performance comparison

Nadezhda Chukhno^{a,*,}, Tomas Bravenec^{b,c}, Javier Díez-González^d, Sergio Trilles^b, Joaquín Torres-Sospedra^e, Antonio Iera^{f,g}, Giuseppe Araniti^{h,g}

^a ICT Faculty, Tampere University, 33014 Tampere, Finland

^b Institute of New Imaging Technologies, Universitat Jaume I, Castellón de la Plana, 12071 Castellón, Spain

^c Department of Radio Electronics, Brno University of Technology, 616 00 Brno, Czechia

^d Department of Mechanical, Computer and Aerospace Engineering, Universidad de León, 24004 León, Spain

^e Departament d'Informàtica, Universitat de València, 46010 València, Spain

^f DIMES, University of Calabria, 87036 Arcavacata di Rende, Italy

^g Consorzio Nazionale Interuniversitario per le Telecomunicazioni (CNIT), 43124 Parma, Italy

^h DIIES Department, University Mediterranea of Reggio Calabria, 89124 Reggio Calabria, Italy

ARTICLE INFO

Keywords:

Cellular networks
Cooperative positioning
Collaborative localization
Device-to-device
Sidelink
Reconfigurable intelligent surfaces
Millimeter wave

ABSTRACT

The next generation of high-accuracy positioning services is required to satisfy the sub-meter accuracy level for more than 95% of the network area, including indoor, outdoor, and urban deployments. In this vein, inter-agent measurements appear to provide additional position information and, hence, have the capacity to boost localization accuracy. This paper researches cooperative positioning techniques by means of device-to-device (D2D) and reconfigurable intelligent surfaces (RIS) technologies leveraging received signal strength (RSS) based ranging. We estimate the maximum capacities of the positioning systems in terms of accuracy through the Gaussian noise model, proposed universal theoretical distance-dependent noise model, and empirical noise model. We also evaluate the positioning error achieved by combining two or more technologies. Numerical results reveal the use cases advantageous for RIS- and D2D-aided localization. Then, based on the results, valuable guidelines are derived on the optimal sensor fusion metric – median – that minimizes the mean error of the cooperative localization.

1. Introduction

1.1. Research motivation

As the fifth-generation (5G) cellular system continues to spread worldwide, researchers are turning their attention to the development of sixth-generation (6G) mobile communication networks [1]. 6G is expected to provide intelligent and ubiquitous wireless connectivity with Terabits per second data rates and sub-millisecond latency over a three-dimensional (3D) network coverage. Acquiring accurate location information from MTs is becoming increasingly critical to achieving these goals, not only for location-based services but also for improving wireless communication performance in various ways, including channel estimation, beam alignment, medium access control, routing, and network optimization [2–4]. To achieve accurate localization and sensing systems, we can expect localization of end devices using 5G/6G technology to exploit D2D [5] and RIS cooperative techniques [6].

Cooperative localization is a technology that holds great promise by providing additional information for positioning through the exploitation of cooperative links between multiple MTs. In D2D-aided cooperative localization, D2D links alleviate the requirement for all MTs to be connected to any of the available base stations (BSs), allowing multi-hop communications among densely located MTs to replace long-range BS-MT communications. Cooperative localization offers more accurate positioning and enhanced coverage compared to noncooperative localization due to the D2D links that have a better SNR and a lower probability of blocked LoS [7].

Indeed, the nLoS problem is one of the most significant challenges in the development of 6G wireless communication systems, which can significantly reduce the accuracy of wireless localization. Despite the potential benefits of using extremely high carrier frequencies, such as millimeter wave (mmWave) and terahertz (THz), and large antenna

* Corresponding author.

E-mail addresses: nadezda.chukhno@tuni.fi (N. Chukhno), bravenec@uji.es (T. Bravenec), jdieg@unileon.es (J. Díez-González), strilles@uji.es (S. Trilles), joaquin.torres@uv.es (J. Torres-Sospedra), antonio.iera@dimes.unical.it (A. Iera), araniti@unirc.it (G. Araniti).

<https://doi.org/10.1016/j.adhoc.2025.103862>

Received 5 August 2024; Received in revised form 24 October 2024; Accepted 8 April 2025

Available online 21 April 2025

1570-8705/© 2025 The Authors. Published by Elsevier B.V. This is an open access article under the CC BY license (<http://creativecommons.org/licenses/by/4.0/>).

arrays, the use of millimeter-scale wavelengths can result in severe path loss, particularly in NLoS scenarios. As a result, the blockage is a major barrier to the widespread adoption of accurate wireless localization systems operating in the mmWave and THz frequency ranges [8]. In this regard, RIS technology can help establish a LoS link between the transmitter and receiver, even in the presence of obstacles or when the power received from the direct path is insufficient for a reliable transmission [9].

Radio positioning involves solving a set of nonlinear equations using various location-related data, including time of arrival (TOA) and angle of arrival (AOA) measurements. The accuracy of these measurements directly affects the overall performance of the positioning process. The total number of available measurements in the system is influenced by factors such as the number of target nodes participating in the process, the number of anchor nodes deployed, and their geometric arrangement. In contrast, the accuracy of the measurements is affected by the signal characteristics and the estimation methods used.

Numerous location estimation techniques have been studied, each possessing unique advantages and drawbacks. Notably, methods such as TOA and time difference of arrival (TDOA) demand strict synchronization, whereas the AOA approach requires complex receiver structures [10,11]. A common challenge associated with these systems is the complexity of the receivers. Many research studies continue to focus on the *simple trilateration* approach, which employs received signal strength (RSS) to mitigate this issue and simplify the receiver's structure [12–14]. RSS is a widely utilized outdoor and indoor localization method that relies on signal propagation measurements, which can be converted into distance measurements provided that suitable path loss models are employed.

In this paper, we investigate cooperative RSS-based localization using D2D and RIS technologies to enhance the localization accuracy in cellular systems by providing a high probability of LoS links. While considerable effort has been devoted to evaluating the performance of D2D and RIS-assisted localization systems individually and their communication performance comparison, a comprehensive analysis of these technologies from a localization perspective and the synergies resulting from their convergence has not been sufficiently explored, despite the potential for new insights for both the research and industrial communities. This forms the basis for the present study.

1.2. Novelty and contributions

To the best of our knowledge, we are the first to (i) provide fundamentals of D2D- and RIS-aided cooperative positioning based on RSS ranging by relying upon the path loss models, (ii) perform their comparison not only from communication perspective but, differently from the state-of-the-art, also from localization ground, and (iii) provide a universal theoretical distance-dependent noise model that can be used, for example, for Cramer-Rao lower bound (CRLB) estimation. Using statistical tools, we also analyze the performance of joint localization integrating cellular, D2D, and RIS cooperative systems. Main contributions of our work are summarized in detail as follows:

- We provide a CRLB procedure that can determine, before real implementation, the maximum capacities of cellular, D2D, and RIS positioning systems in terms of accuracy. Also, usually, CRLB considers only white Gaussian noise. We take into account LoS/nLoS conditions and distance-dependent 3GPP-compliant noise models as well;
- Noise and sometimes nLoS are typical uncertainties. However, noise models from the literature depend on several pre-established parameters (e.g., LoS probability) and can only be applied in certain environments. Our proposed theoretical distance-dependent noise model is universal for all technologies and all scenarios defined in 3GPP. In this case, the path loss equations and LoS probability should be recalculated for every environment based on distance. We compare the proposed theoretical model against the intuitive empirical one usually used in ray tracing algorithms;

- We provide comprehensive D2D- and RIS-aided cooperative localization comparison using ranging technique. In addition, we offer a summary of their comparison from a communication perspective in Section 2.3;
- We provide a collection of localization equations for D2D- and RIS-aided¹ positioning in a unified terminology, along with the necessary context and materials to ensure the reproducibility of the simulations;
- We propose a novel approach to integrate D2D and RIS communication model into positioning algorithms by using the statistical mean and median for sensor fusion at the location-level;
- We identify relevant use cases for RIS-aided localization and RIS communications in general.

The rest of the paper is organized as follows. In Section 2, we review the related works and identify research gaps. Section 3 introduces main localization principles, starting with our system models based on RSS measurements for D2D- and RIS-aided localization and the relevant path loss models, and discusses trilateration, triangulation and fingerprinting methods. In Section 4, we provide the CRLB formulation with Gaussian noise as well as propose a new theoretical distance-dependent noise model. In Section 5, the numerical results and discussion are presented, where we compare the results for different CRLBs and conduct the performance analysis of D2D- and RIS-aided cellular localization in terms of positioning accuracy. Conclusions are drawn in Section 6.

2. Related works

2.1. D2D-based cooperative positioning

A cooperative D2D-aided method has been explored as a means to improve the localization accuracy, which can be performed in two ways to facilitate localization: (i) pseudo-range estimation and (ii) location information exchange [15]. In the former case (that is in widespread use by researchers), when direct D2D communications over the sidelink (also named PC5 interface) are exploited, MTs inherently receive signals from each other, which provide additional reference signals and may thus be utilized to compute pseudo-range estimations between MTs. In the latter case, the direct exchange of necessary data between MTs can be performed; both common physical layer estimates (to speed up the local decisions) and position information are exchanged over D2D links to enhance the accuracy of the localization system.

In [16], a collaborative method using only direct communication to nearby devices and fingerprinting is introduced to enhance indoor positioning accuracy. The approach verifies the fingerprinting positioning by TOA-based distance passed through the D2D links. Similarly, in [17], the advantages of direct communication between nodes in the case of 5G internet of things (IoT) applications are proven to achieve the sub-meter localization accuracy and enhance coverage. In [18], a positioning system for smartphones based on the received strengths of WiFi and Bluetooth signals is presented. The additional signal strength information of Bluetooth signals exchanged between D2D users is used to estimate their relative distances, thereby decreasing the error of the position estimates.

Similarly, in [19], radio frequency (RF)-sensing with new radio (NR) sidelink D2D communication integration is studied to achieve device-initiated, flexible sensing capabilities in beyond 5G cellular communication systems. In [20], the pseudo-range estimates, such as TDOA, between MTs are used to empower cooperative positioning in 5G high-density networks. Authors show that at densities greater than 1100 MT/m², sub-meter positioning accuracy can be provided with the outage probability converging to zero. In [21], a beam sweeping

¹ There is no theoretical basis in the literature on RIS-aided positioning systems based on RSS ranging.

Table 1
RISs vs. relays: communication perspective.

Advantage	RIS	Relay
Spectral efficiency [26–29]	✓ (with large surface area)	✓ (full duplex)
Noise [26,27,29]	✓ (not affected by addicted noise, no self-interference)	× (affected)
Energy efficiency [30]	× (except when very high rates are required)	✓
Signal range [28]	× (reduced signal range due to the lack of amplification)	✓
SNR (Fig. 1)	×	✓
Power budget [27]	✓	× (power sharing between BS & relay)
Power consumption [27,28]	✓ (use of printed metamaterial requires no amplifiers)	×
Hardware complexity/cost [27,28]	✓ (lower complexity)	×

approach for TOA and AOA measurements stemming from the defined and regulated procedures for NR beam management is considered. It is shown that joint angle- and time-based measurements allow for reaching sub-meter accuracy and a relatively robust system against different node geometries.

Differently, in [22], cooperative RSS-based localization is used for interference avoidance in a cognitive radio network. In [23], a collaborative indoor positioning system using multilayer perceptron neural networks is proposed to improve the accuracy of the models based on bluetooth low energy (BLE) and RSS lateration and cope with inappropriate anchors' distribution, unstable RSS, and hardware heterogeneity.

Although many research works have focused on D2D cooperative positioning performance evaluation and experiments, the literature still lacks mathematical models [15,16,24].

2.2. RIS-based cooperative positioning

5G radio for mmWave and beyond-5G concepts at 0.1 THz to 1 THz can exploit time-, power-, and angle-based measurements for localization by taking advantage of large available bandwidth and antenna arrays. However, obstacles can block the signals, thereby causing large positioning errors. RISs are regarded as one of the foremost technologies capable of controlling the physical propagation environment. They are embedded by passively reflecting radio waves in desired directions and actively sensing this environment in both receive and transmit directions [25].

RIS is commonly used as a reflector and can operate in two ways. First, it can function as part of the passive environment, acting like any other scatterer or reflector. Second, it can serve as part of the infrastructure, acting as a global reference or anchor point [31]. The potential of RIS for localization has been given limited attention in the literature [31]. In [25], a multi-user RIS-enabled localization problem is examined, and the users' position in 3D space is estimated by calculating the TOA of the LoS and nLoS paths at multiple receivers. An adaptive phase shifter design based on hierarchical codebooks and feedback from the MT is proposed in [32] for joint positioning and communication in RIS-aided mmWave multiple-input and multiple-output (MIMO) systems. Differently, in [33], RIS is used as a means of blockage mitigation and channel state information acquisition for a RIS-aided mmWave system through 3D positioning.

In general, RIS technology provides many advantages over existing mainstream technologies [34]. However, the central question that can stimulate the practical RIS development of “*what is a convincing use case for RIS?*” remains unanswered [28]. Coverage expansion is one possibility, but traditional half-duplex relaying is a viable alternative, and full-duplex regenerative relays are emerging [35]. In comparison to wideband channels, RIS technology faces a competitive disadvantage due to the requirement of identical programming for each RIS element over the entire frequency range. Another potential use case is enhanced spatial multiplexing and interference reduction, but it must compete with cell-free MIMO systems. The effectiveness of RIS technology may be greatest in THz regions, where the development of coherent transceivers is challenging due to the sparse channels that make additional propagation paths crucial, even if they are of poor quality. However, so far, there is no evidence, only guesses [28].

In this study, we strive to fill the mentioned gap by answering the question of *what are convincing use cases for RIS-aided localization.*

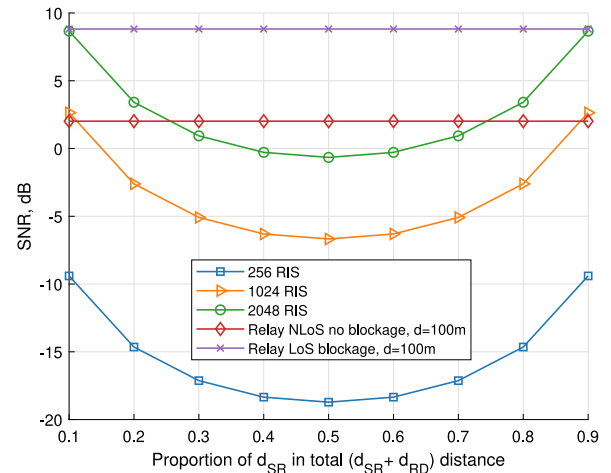


Fig. 1. SNR comparison of RIS and relays. On the x-axis is the proportion of d_{SR} and d_{RD} distances when $d_{SR} + d_{RD} = 100$ m. For example, x-axis of 0.1 means that RIS is located such that $d_{SR} = 10$ m and $d_{RD} = 90$ m.

2.3. RISs vs. relays

When examining the current research works on the comparison between RIS and D2D performance, it is evident that existing studies primarily concentrate on spectral efficiency, complexity, and energy efficiency, among other relevant metrics (see Table 1). First, it is essential to emphasize the spectral efficiency advantages of RIS compared to D2D when its size is substantially larger than the wavelength [26–28]. Moreover, RIS operates in a full-duplex mode without self-interference or introducing thermal and addictive noise since passive RIS cannot amplify or regenerate the signals. Consequently, they may achieve higher spectral efficiency than active half-duplex relays.

A system that can switch between single-input single-output (SISO) and decode-and-forward relaying modes is generally preferred to minimize the transmit power and maximize the energy efficiency, except when very high data rates are required. In such cases, when the data rate exceeds $8.48 \text{ bit s}^{-1} \text{ Hz}^{-1}$ [30], RIS may be a better option in terms of energy efficiency. However, RIS has the drawback of a reduced signal range [28] owing to its passive nature and lack of amplification, which can result in a lower SNR.

In Fig. 1, we provide a visual representation of the SNR in relation to the proportion of distance d_{SR} between the source –S– (i.e., BS) and RIS to the total propagation $d_{SR} + d_{RD}$ distance (i.e., path BS-RIS-MT, or source-RIS-destination –D–) of 100 m. We also display the relay's SNR for the given distance of 100 m between devices for blockages by both large-scale and small-scale constructions (i.e., nLoS non-blocked and LoS blocked by the human body). It is evident from the figure that only large-size RISs can achieve comparable performance to the relays when placed either close to the source or the destination. It is worth noting that distances between relays are typically smaller than 100 m, implying that the SNR of the channel between relays would be even higher in such cases.

Table 2
State of the art comparison.

Work	Year	Approach	Area	Environment	Benchmark	Metric	Accuracy	RIS vs. D2D
[20]	2015	D2D communication cooperative positioning with different device density	D2D range \approx 50 m, BS range 100 m to 400 m	General	CRLB	95th PRC	From 50 cm to 100 m	×
[36]	2021	1 RIS, 1 BS, 1 user positioning	20 m \times 20 m	Indoor	CRLB, GDoP, no RIS	position error bound (PEB)	Achieve up to two orders of magnitude reduction in PEB (compared to no RIS)	×
[37]	2022	Get relative location of MT with respect to RIS. Then through D2D, distances between MTs are calculated	100 m \times 80 m	General	Non cooperative	RMSE	2 m to 22 m depending on the number of beams	×
[38]	2022	Zero access points positioning: two MTs estimate their positions through D2D communications, and processing the signals reflected from RIS	20 m \times 17 m	General	CRLB	PEB	Sub-meter accuracy	×
[39]	2023	Zero access points positioning: at least three half-duplex single-antenna devices and a single RIS as anchors	7 m \times 7 m \times 4 m	Indoor	CRLB	RMSE	Centimeter-level accuracy at 20 dBm transmission power	×
[40]	2024	RIS as anchors for cooperative localization: RIS phase shift control optimization algorithm	30 m \times 30 m \times 5 m	Indoor	Alternate optimization, genetic algorithm	Squared PEB	Error of proposal is 94.68% smaller than when using sensor nodes as anchors	×
Our work	2024	Comparison of D2D- and RIS-based positioning systems in terms of accuracy based on simple ranging approach	100 m \times 100 m	General	CRLB	Range of metrics	See Section 5. Under equal placement, D2D can improve cellular positioning by 47% and RIS by 38%	✓

In relay-assisted systems, the power budget limitation is generally ensured by allocating the total RF power between the transmitter and the relay to meet the total power constraint. Conversely, in the ideal scenario, the total power reflected by a RIS is equal to the total power of the incident radio waves [27]. Additionally, utilizing printed meta-materials eliminates the need for amplifiers, which is beneficial for energy consumption [27,28].

Furthermore, the noteworthy benefit of RISs is the reduction in hardware complexity (e.g., with analog beamforming, no extra RF chains needed for demodulation and modulation) at the expense of a larger surface area [28]. Additionally, RISs are semi-passive devices with a relatively low cost, which makes them ideal for mounting on surfaces or moving objects [25].

In contrast to what is commonly done in the literature, we aim to compare the localization accuracy of RIS- and D2D-assisted localization systems in Section 5.

2.4. State of the art of cooperative positioning

Within the existing literature, one can encounter papers that introduce positioning algorithms based on D2D technology, those based on RIS technology, as well as those that explore a combination of both approaches, as shortly reported in Table 2. However, this particular study distinguishes itself by not proposing a novel algorithm. Instead, our focus lies in the comparative analysis of existing technologies, specifically D2D and RIS, with regard to their positioning accuracy. Through this work, our goal is to present a comprehensive assessment of these technologies' positioning accuracy while using simple ranging. By leveraging the outcomes of this research, both scholars and industry professionals can make informed decisions regarding the appropriate contexts for employing either D2D, RIS, or a synergistic fusion of both solutions.

3. System model

This section presents D2D- and RIS-aided localization models that rely on RSS ranging while taking into account a general path loss model. A list of notations used in this paper is provided in Table 3.

Assumption 1. Our analysis pertains to an environment challenging for localization due to the scattered deployment of beacons. In such a context, cooperation among peers can enhance the accuracy of the system.

Assumption 2. One user lacks access to the localization system, but he can estimate the position by utilizing information provided by peers/RISs as a part of the infrastructure.

Localization aims to find the 3D coordinates of specific targets. To do so, it is essential to have at least four beacon nodes in wireless communication networks. Positioning algorithms typically rely on range measurements, including methods such as RSS, TOA, AOA, and TDOA [41]. Generally, positioning-related measurements are categorized into four main classes:

- Time-based (e.g., TOA, TDOA, round-trip time);
- Angle-based (e.g., AOA, angle of departure);
- Power-based (e.g., RSS, backscattered power) using path loss models;
- Frequency-based (e.g., frequency of arrival (FOA), and frequency difference of arrival (FDOA)).

Localization methods commonly used to determine positions include fingerprinting and geometry-based triangulation and trilateration (see Fig. 2). Fingerprinting is a technique where a database of “fingerprints” of signal characteristics (i.e., signal strength, time of arrival)

Table 3
Symbology and notation used in the manuscript.

Communication	
W	Available bandwidth, Hz
f_c	Carrier frequency, GHz
d_{2d}	Two-dimensional distance between MT and NR BS, m
d	Three-dimensional distance between MT and NR BS, m
P_T, P_R	Transmit/received power, W
G_T, G_R	Transmit/received antenna array gains, dBi
N_0	Power spectral density of noise, dB/Hz
$L(d)$	Path loss in linear scale
$L_{dB}(d)$	Path loss in decibel scale
A, ζ	Propagation exponents
$p_B(d)$	Distance-dependent blockage probability
w	Shadow fading, dB
σ_{SF}	Standard deviation of noise
p_L	LoS probability
Localization-specific parameters	
m	Measurements
d	Distance
n	Noise
α_i	Constant term which takes into account the transmission power of the node to be localized (propagation coefficient)
$L_{dB}(d_0)$	Path loss at the reference distance d_0 in decibels
d_0	Reference distance, m
(x, y, z)	Unknown coordinates
(x_i, y_i, z_i)	Position coordinates of anchor i
\hat{d}_i	Calculated distance from anchor i
$RSSI_i$	Received power from anchor i
RIS-specific parameters	
d_{SR}	Distance from BS to RIS, m
d_{RD}	Distance from RIS to MT, m
$L(d_{SR})$	Path loss of sub-path from BS to RIS
$L(d_{RD})$	Path loss of sub-path from RIS to MT
Γ_k	Reflection coefficient of the k -th RIS element
L_{TOT}	Total path loss of a RIS
$L_{TOT}(d_0)$	Total path loss of a RIS at the reference distance d_0
$M \times N$	Sub-wavelength elements of RIS
$s_M \times s_N$	Size of sub-wavelength elements of RIS
dm, n	Distance between the BS and the (m, n) -th RIS element
dm, n	Distance between the (m, n) -th RIS element and the MT
$P_{R,k}$	Received power in watts at the MT through the k -th RIS element
φ_k	Phase difference induced by k -th RIS element
G_i^e	Gain of the RIS in the direction of an incoming wave
G_r^e	Gain of RIS in the direction of a received wave
e_b	Efficiency of RIS
ϕ_k	Phase delay of the signal received through k -th RIS element

is created for various locations in the environment. When the MT captures the signal characteristics at its location, it compares them to the fingerprints in the database to determine its position. Triangulation/trilateration involves determining the position of an MT by measuring the angles/distances, respectively, between the target MT and multiple known anchors. Triangulation estimates the target MT's position based on the intersection of these angles by using the principles of trigonometry and knowing the distances or relative positions of the anchors. Similarly, trilateration calculates the MT's position based on the intersection of spheres or circles in 3D or 2D space, respectively.

These methods offer different approaches to determine the position of an MT, each with its own strengths and limitations. A primary limitation of fingerprinting is the requirement for a database of reference samples, which may not always be feasible to collect [42]. Geometry-based techniques require at least three anchors with known positions and underlining models to map measurements into distances. In certain scenarios, locating the necessary anchors can be challenging, making the use of a database with fingerprinting a more viable and reliable approach. In general, the choice of method depends on factors such as the available infrastructure, the accuracy requirements, the nature of the environment, and the specific application in which localization is needed.

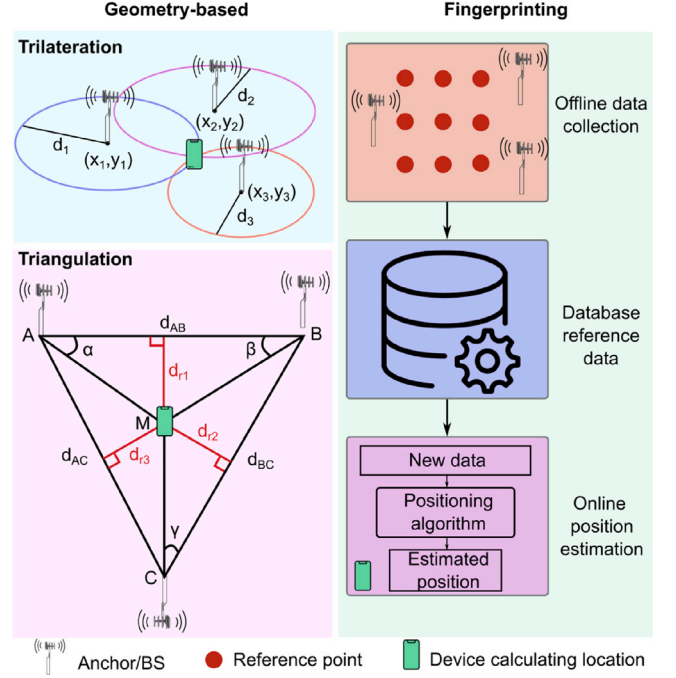


Fig. 2. Illustration of main localization principles.

3.1. D2D-aided localization using power measurements

In this subsection, we will discuss power-based measurements. Since RSS decreases based on path loss models, we can create a general model to convert power measurements m into distance using the equation below:

$$m = f(d) + n, \text{ hence, } d \approx f^{-1}(m), \quad (1)$$

where $f(\cdot)$ corresponds to the model function, n represents noise, and m represents the obtained measurements.

Among the various channel models proposed for both indoor and outdoor settings (e.g., Nakagami, Rayleigh, Rician, etc.) [43], the most commonly used one for radio frequency signal-based localization is the simple lognormal shadowing path loss model, which illustrates the following relationship between the received power and the distance between the transmitter and receiver [44–46]:

$$RSSI(d, Bm) = \alpha_i(d, Bm) - 10\zeta \log(d) + w, \quad (2)$$

where α_i is a constant term representing the propagation coefficient of the transmitted power, d signifies the distance between the transmitter and receiver, ζ corresponds to path loss exponent (PLE), and w is a zero-mean Gaussian random variable.

$$w[dB] \sim \mathcal{N}(0, \sigma_{SF}^2), \quad (3)$$

where σ_{SF}^2 corresponds to the standard deviation specified for various propagation environments in Table 4.

Denote $\alpha_i = P_r(d_0)$:

$$\alpha_i = P_T + G_T + G_R - L_{dB}(d_0), \quad (4)$$

where P_T represents the transmit power, G_T and G_R denote the transmit and receive antenna gains respectively, and $L_{dB}(d_0)$ corresponds to the path loss at a reference distance of d_0 (usually, $d_0 = 1$ m).

The distance between the MT and BS i (or between the MT and relay i) can be determined using expression:

$$\hat{d} = 10^{\frac{\alpha_i - RSSI_i + w}{10\zeta}}. \quad (5)$$

Table 4
Propagation models [47–49].

Environment	PLE, ζ	SF, σ_{SF}^2	$L_{dB}(d_0)$, non-blocked	$L_{dB}(d_0)$, blocked
3GPP Indoor, InH - Office LoS	1.73	3	$32.4 + 20 \log_{10} f_c$	$47.4 + 20 \log_{10} f_c$
3GPP Indoor, InH - Office nLoS	3.19	8.29	$32.4 + 20 \log_{10} f_c$	$47.4 + 20 \log_{10} f_c$
mmMAGIC UMi Street Canyon LoS	1.92	2	$32.9 + 20.8 \log_{10} f_c$	$47.9 + 20.8 \log_{10} f_c$
mmMAGIC UMi Street Canyon nLoS	4.5	7.82	$31 + 20 \log_{10} f_c$	$46 + 20 \log_{10} f_c$
5GCM UMi Open Square LoS	1.85	4.2	$32.4 + 20 \log_{10} f_c$	$47.4 + 20 \log_{10} f_c$
5GCM UMi Open Square nLoS	2.89	7.1	$32.4 + 20 \log_{10} f_c$	$47.4 + 20 \log_{10} f_c$
3GPP UMi Street Canyon LoS	2.1	4	$32.4 + 20 \log_{10} f_c$	$47.4 + 20 \log_{10} f_c$
3GPP UMi Street Canyon nLoS	3.19	7.82	$32.4 + 20 \log_{10} f_c$	$47.4 + 20 \log_{10} f_c$
3GPP UMa LoS	2.2	4	$28 + 20 \log_{10} f_c$	$43 + 20 \log_{10} f_c$
3GPP UMa nLoS	3	7.8	$32.4 + 20 \log_{10} f_c$	$47.4 + 20 \log_{10} f_c$

The following is the quadratic equation for the 3D trilateration localization algorithm:

$$\hat{d}_i = \sqrt{(x_i - x)^2 + (y_i - y)^2 + (z_i - z)^2}, \quad (6)$$

where, (x, y, z) represents the estimated target MT coordinate, while (x_i, y_i, z_i) denotes the position of the anchors. The calculated distance from the target mt to anchor i is denoted by \hat{d}_i . Since there are four equations with three unknown variables, any three equations from (6) with $i = 1, \dots, 4$ can be used to determine the unknowns. In practical situations, the calculated distances may not always be accurate. Consequently, four reference points are used to estimate the target MT coordinate.

Our research investigates the building and the human body blockage in relation to LoS/nLoS states, which encompass both outdoor and indoor settings like city streets, plazas, arenas, and offices, among others. For instance, in a manner similar to [50], we can consider a scenario where the state of the MT falls into one of the four possible states: (LoS, blocked), (LoS, non-blocked), (nLoS, blocked), (nLoS, non-blocked). In this context, the nLoS state means that buildings can obstruct the path between the BS and the MT, while the blocked state presumes a human blockage of 15 dB [51].

Then, the path loss, measured in decibels (dB), for the four states is given by the following equation:

$$L_{dB}(d) = L_{dB}(d_0) + 10\zeta \log_{10} d, \quad (7)$$

where d is the three-dimensional distance between the mmWave BS and the MT, or between two MTs, f_c is the frequency of the carrier in GHz, while PLE ζ and reference path loss $L_{dB}(d_0)$ depend on the radio environment. The PLE, standard deviation values, as well as path loss equations depending on the used model, are provided in Table 4.

The likelihood of LoS probability p_L for the 2D distance d_{2D} between the NR BS and the mobile terminal MT, along with the distance between the two MTs, can be calculated using propagation models as described in [47–49] (see Fig. 3). On the other hand, the probability of human blockage at a 3D distance d is derived in [52].

The equation for path loss utilizing the model in linear scale can be expressed as $L(d) = Ad^\zeta$, where A and ζ correspond to the propagation coefficients, and $A = 10^{\frac{L_{dB}(d_0)}{10}}$.

3.2. RIS-aided localization using power measurements

Here, we adopt the notion of reflection unit set (RUS) presented in [33] and calculate \hat{d}_i for each RUS, $i = 1, \dots, 4$. With four specific RUSs serving as anchor nodes placed in known locations, coordinates $p_1 = (0, 0, 0)$, $p_2 = (0, a, 0)$, $p_3 = (0, a, b)$, and $p_4 = (0, 0, b)$ (where both a and b are real values), the position of the MT is not known, but it is represented by (x, y, z) , and the measured distances between each anchor and the MT are denoted by d_i , respectively. The actual distances are defined based on these measurements as:

$$\hat{d}_1 = \sqrt{x^2 + y^2 + z^2}, \quad (8)$$

$$\hat{d}_2 = \sqrt{x^2 + (y - a)^2 + z^2}, \quad (9)$$

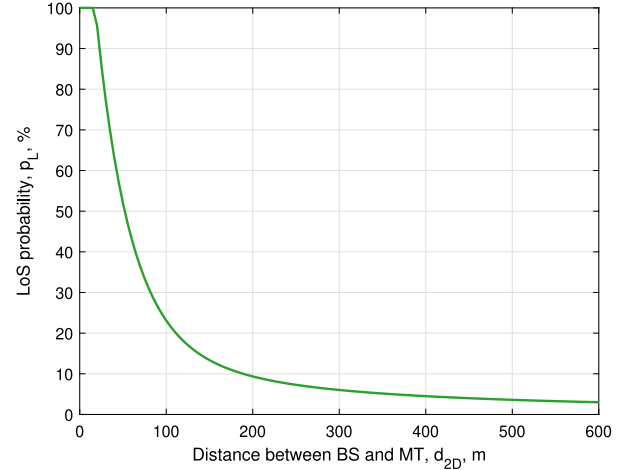


Fig. 3. LoS probability as a function of 2D distance between the BS and the MT according to 3GPP UMi Street Canyon model from [47].

$$\hat{d}_3 = \sqrt{x^2 + (y - a)^2 + (z - b)^2}, \quad (10)$$

$$\hat{d}_4 = \sqrt{x^2 + y^2 + (z - b)^2}. \quad (11)$$

The three unknown variables (x, y, z) can be determined by solving the four equations. These variables are crucial in both clock synchronization and antenna array, which have stringent requirements for accuracy and precision.

When measuring the power of the cascaded BS-RIS-MT channel, the distance can be calculated using:

$$\alpha_i = P_T + G_T + G_R + |I_i| - L_{TOT}(d_0), \quad (12)$$

where I_i and L_{TOT} are defined lower in this section. The distance between the MT and BS i is then calculated using:

$$d = 10^{\frac{\alpha_i - RSSI_i + w}{10\zeta}} - d_{SR}, \quad (13)$$

where RSSI is calculated using (16) and the distance between the BS and the RIS is denoted by d_{SR} , which is a known quantity.

Assumption 3 ([53]). The RIS consists of $M \times N$ sub-wavelength elements, each with the size of $s_M \times s_N$. It is assumed that $D_{m,n}$ represents the distance between the (m, n) th RIS element and the BS, while $d_{m,n}$ is the distance between the (m, n) th RIS element and the MT. The distances from different RIS elements to the BS are approximately the same, i.e., $D_{m,n} \approx d_{SR}$, where d_{SR} represents the distance between the BS (i.e., source) and the center of the RIS.

The path loss models presented in Table 4 are employed to express the path loss of sub-paths $L(d_{SR})$ and $L(d_{RD})$ from source to RIS and from RIS to destination, respectively. Total received power in watts at the MT through the k th RIS element is computed under the plate

scattering paradigm [54]:

$$P_{R,k} = \frac{P_T |\Gamma_k| G_T G_R}{L(d_{SR})L(d_{SR})}, \quad (14)$$

where $L(d_{SR})$ and $L(d_{RD})$ are path losses at distances d_{SR} and d_{RD} , correspondingly, Γ_k is the reflection coefficient of the k th RIS element:

$$\Gamma_k = e^{-j\varphi_k} G_i^e G_r^e \epsilon_b, \quad (15)$$

where φ_k is the phase difference induced by k th RIS element, G_i^e is the gain of the RIS in the direction of an incoming wave, G_r^e is the gain of RIS in the direction of a received wave, and ϵ_b is the efficiency of RIS, which is defined as a ratio of transmit signal power by RIS to received signal power by RIS. We assume that RIS consists of **passive elements** and $\epsilon_b = 1$.

Total received power at the receiver, including all RIS elements, is given by

$$P_R = \left(\sum_k \sqrt{\frac{P_T |\Gamma_k| G_T G_R}{L(d_{SR})L(d_{RD})}} e^{j\phi_k} \right)^2, \quad (16)$$

where ϕ_k is the phase delay of the signal received through k th RIS element.

Assumption 4 ([55]). For the sake of simplicity, we assume that RIS elements reflect signal with unit-gain reflection coefficients (i.e., $|\Gamma_k| = 1$) and in such a way that all the signals coming through different RIS elements are in phase at the receiver (i.e., $\phi_k = \varphi_k$).

Then, expression (16) becomes:

$$P_R = \left(\sum_k \sqrt{\frac{P_T G_T G_R}{L(d_{SR})L(d_{RD})}} \right)^2. \quad (17)$$

Hence, the total path loss is expressed as

$$L_{TOT} = \left(\sum_k \sqrt{\frac{1}{L(d_{SR})L(d_{RD})}} \right)^{-2}. \quad (18)$$

3.3. Localization using angle measurements

In this subsection, we review the triangulation method. Given the known AOAs, α , β , known distance d_{AB} between two anchors (see Fig. 2), intermediate distance d_{r1} that forms a right angle triangle can be extracted from

$$d_{AB} = \frac{d_{r1}}{\tan \alpha} + \frac{d_{r1}}{\tan \beta}, \quad (19)$$

by using well-known trigonometric identities:

$$d_{r1} = d_{AB} \frac{\sin(\alpha + \beta)}{\sin \alpha \sin \beta}. \quad (20)$$

Therefore, distance d_{AM} between the first anchor and MT can be found using basic trigonometric functions as

$$d_{AM} = \frac{d_{r1}}{\sin \alpha}. \quad (21)$$

In a similar fashion, distances d_{BM} and d_{CM} between the other two anchors and MT can be obtained using angle γ and distances d_{AC} and d_{BC} . The MT's position can be derived from the intersection of the three calculated distances (i.e., d_{AM} , d_{BM} , and d_{CM}) while knowing the coordinates of the corresponding anchors.

3.4. Choice of positioning method

Trilateration is widely preferred for position estimation due to its simplicity compared to other methods such as triangulation. Fingerprinting, on the other hand, is more specific to the environment and typically relies on a reference database, making it more suitable for experimental studies. In the upcoming section, we will primarily focus on utilizing trilateration for our position estimation.

4. Cramér–Rao lower bound

4.1. CRLB with Gaussian noise [56]

The CRLB serves as a metric for measuring the minimal theoretical estimation errors attainable by an estimator. Assuming $\mathbf{p} = [x, y]^T$ represents the vector of parameters to be estimated (i.e., the target position), and $\boldsymbol{\rho} = [\rho_1, \dots, \rho_n]^T$ represents the vector of ideal measurements influenced by zero-mean Gaussian uncertainties $\boldsymbol{\eta} = [w_1, \dots, w_n]^T$, where $\text{cov}(\boldsymbol{\eta}) = E\{\boldsymbol{\eta}\boldsymbol{\eta}^T\}$ denotes the covariance matrix and w is defined in Eq. (3), with n denoting the number of anchors, the CRLB is expressed as per [57]:

$$CRLB = (\mathbf{H}^T \text{cov}(\boldsymbol{\eta})^{-1} \mathbf{H})^{-1}, \quad (22)$$

where

$$\mathbf{H} = \begin{bmatrix} \lambda_{x_1}(\mathbf{p}) & \lambda_{y_1}(\mathbf{p}) \\ \lambda_{x_2}(\mathbf{p}) & \lambda_{y_2}(\mathbf{p}) \\ \vdots & \vdots \\ \lambda_{x_n}(\mathbf{p}) & \lambda_{y_n}(\mathbf{p}) \end{bmatrix}, \quad (23)$$

being $\lambda_{x_i}(\mathbf{p}) = (x - X_i/\rho_i)$ and $\lambda_{y_i}(\mathbf{p}) = (y - Y_i/\rho_i)$ the first derivatives of $\rho_i = h_i(\mathbf{p}) = \sqrt{(x - X_i)^2 + (y - Y_i)^2}$ for the i th ranging measurements, $\mathbf{a}_i = [X_i, Y_i]^T$ is i th anchor's position.

4.2. CRLB with distance-dependent noise

In this subsection, a noise variance distance-dependent model associated with 3GPP path loss models is implemented. Since we use RSS-based ranging and trilateration method based on distance, therefore, the variances expressions for noise and nLoS have the following form [58]:

$$\eta_i = \frac{c^2}{W^2 (P_T/P_n)} L_i, \quad (24)$$

where η_i is the receptor range estimate variance, $\boldsymbol{\eta} = [\eta_1, \dots, \eta_n]^T$, c is the pulse propagation velocity, W is the bandwidth, P_T is the transmit power, and P_n is the power density of noise.

We propose a theoretical (probabilistic) approach to quantify the path loss for distance-based noise variances:

$$L_i = L_{LoS}(d)p_L + L_{nLoS}(d)(1 - p_L), \quad (25)$$

where LoS and nLoS probabilities, p_L and $(1 - p_L)$ respectively, reflect the likelihood of a direct visible path between transmitter and receiver. This probabilistic model accounts for the varying noise characteristics in LoS and nLoS scenarios, providing a comprehensive representation of the overall noise in telecommunication systems. The model is 3GPP compliant, which means that only path loss equations (defined in Table 4) and LoS probability should be recalculated depending on the environment.

On the other hand, we also provide an empirical approach to describe distance-based noise (path loss component). Empirically,

$$L_i = L_{LoS}(d_{LoS}) + L_{nLoS}(d_{nLoS}), \quad (26)$$

where both $L_{LoS}(d_{LoS})$ and $L_{nLoS}(d_{nLoS})$ path losses are considered functions of distance, capturing the empirical relationship between the distance separating communication nodes and the resulting noise levels.

The theoretical approach, as outlined in Eq. (25), offers a distinct advantage in its universality. It allows for the estimation of path loss by leveraging distance d and LoS probability p_L . In contrast, the empirical approach (26) ensures that path loss is computed separately for both the LoS (d_{LoS}) and nLoS (d_{nLoS}) segments of the distance d . This necessitates making assumptions regarding LoS probability (unless leveraging ray-tracing algorithms).

In Fig. 4, we provide the results for theoretical and empirical approaches to model distance-dependent noise variances. One may

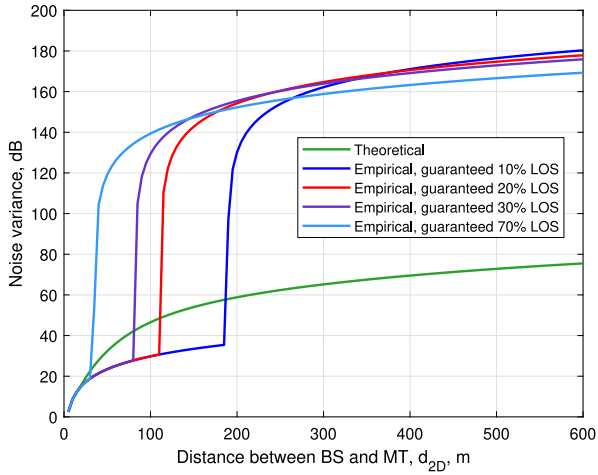


Fig. 4. Visualization of distance-dependent noise variances, 3GPP UMi Street Canyon LoS/nLoS.

observe that the empirical noise variance depends on the probability of guaranteed LoS conditions presented earlier in Fig. 3. At the beginning of each curve, for the distance guaranteed to be LoS, the noise variance remains low, as expected in LoS scenarios. However, this trend faces a sudden growth when the distance is no longer guaranteed to be in LoS. On the other hand, the theoretical representation of the distance-dependent noise variance grows steadily with increasing distance, following a logarithmic trend without any deviation from this trend.

5. Numerical results

This section introduces the evaluation of D2D- and RIS-cooperative localization systems across various scenarios, specifically for the 3GPP UMi Street Canyon use case considering LoS and nLoS conditions. A single path loss model is used as it ensures a fair comparison between the two technologies by keeping a consistent and well-known propagation model. We anticipate that using other alternative models would yield similar trends and conclusions with minor differences. Therefore, for conciseness and without compromising generality, we focus on the 3GPP UMi Street Canyon scenario while varying the positions and geometries of the anchors. With this anchor placement strategy, we provide heterogeneous device deployments.

5.1. Simulation setup and section organization

We conduct our simulations using MATLAB environment and publish open-source code as indicated in Section 6. We note that our positioning framework is validated via simulations, being a widely adopted approach and indispensable tool for researchers in this domain due to the lack of RIS-related hardware. In the **cellular positioning** scenario, we consider the service area of $100\text{m} \times 100\text{m}$, where the four BSs are located at its corners (see Fig. 5). The coordinates of BSs therefore are $(0, 0)$, $(0, 100)$, $(100, 100)$, and $(100, 0)$. For **RIS-aided positioning**, RISs are placed close to the BSs for effective operation (e.g., with a BS-RIS distance of approximately 10m) [55], as discussed in Section 2.3. The coordinates of RISs are $(7.1, 7.1)$, $(7.1, 92.9)$, $(92.9, 92.9)$, and $(92.9, 7.1)$. The locations of the relays (i.e., D2D anchors) may vary depending on the scenarios (see Fig. 5). Specifically, the following options are possible:

- relays have the same coordinates as RISs;
- relays are uniformly distributed within the service area;

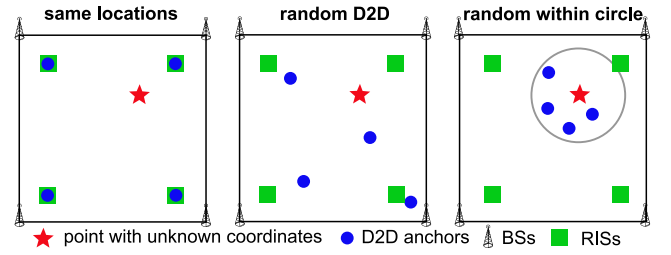


Fig. 5. Visualization of devices deployments: considered use cases.

- relays are uniformly distributed within an area delimited by a circle with a radius of 20m and centered in the point with unknown coordinates.

In **relay-aided systems**, the total RF power is typically split between the transmitter and the relay to maintain a fixed power budget. Moreover, using a full-duplex (FD) relaying protocol introduces high loop-back self-interference (I_S) at the relay due to the simultaneous transmission and reception of signals.

As the main error measurement, we use the Euclidean distance between the estimated position and the current one (i.e., ground truth). We have selected the main evaluation metrics according to the ISO18305 standard [59] and the EvAAL/IPIN Indoor Localization Competition [60]. Thus, we provide the mean, median, and standard deviation as well as minimum, maximum, 75th, and 95th percentile of the positioning errors over the L evaluation points and the rep repetition times. We complement them with the mean squared error (MSE) (27) and the root mean squared error (RMSE) (28), as they penalize the presence of large outliers in the obtained positioning errors.

$$MSE = \frac{1}{L} \sum_{l=1}^L (x_l - \hat{x}_l)^2 + (y_l - \hat{y}_l)^2, \quad (27)$$

$$RMSE = \sqrt{\frac{1}{L} \sum_{l=1}^L (x_l - \hat{x}_l)^2 + (y_l - \hat{y}_l)^2}, \quad (28)$$

where l stands for the l th evaluation point, L is the number of evaluation points, (x_l, y_l) is the real position, (\hat{x}_l, \hat{y}_l) is the position estimate.

Within our experimental setup, we sample $L = 30$ evaluation points at random locations and measure the positioning accuracy 1000 times per point. With this approach, we warrant that different random initializations have been considered. In our cooperative positioning method, we fused the position obtained from the different technologies by applying a simple centroid-based loose coupling approach. The final estimate (\hat{x}, \hat{y}) corresponds to the unweighted centroid (i.e., the plain average of coordinates) cellular and D2D positioning. That is:

$$\hat{x} = \frac{\hat{x}^{cel} + \hat{x}^{d2d}}{2}; \hat{y} = \frac{\hat{y}^{cel} + \hat{y}^{d2d}}{2}. \quad (29)$$

The organization of this section is as follows. We first provide the theoretical lower bounds results gained through the CRLB, focusing on each technology and different noise models. We then begin with investigating cooperative positioning methods on a simple LoS scenario for UMi Street Canyon with a known PLE of $\zeta = 2.1$ and $\sigma_{SF}^2 = 4$ in Sections 5.3–5.5, for equal placement of RISs and relays, random placement of relays, and random placement of relays within 20m radius, respectively. Then, we investigate the impact of nLoS conditions on D2D and cellular positioning for UMi Street Canyon with $\zeta = 3.19$ and $\sigma_{SF}^2 = 7.82$ in Section 5.6, while RIS technology preserves an assumption of LoS operation only. Finally, we summarize all the results in Section 5.7. Table 5 provides the parameters for the performed simulations.

Table 5
Default parameters.

Parameter	Value
Carrier frequency, f_c	28 GHz
Transmit power (BS), P_T	20 dBm [61]
Operating bandwidth, W	100 MHz
Transmit power (relay), $P_T/2$	10 dBm
Noise spectral density, N_0	-174 dBm/Hz
Self-Interference, I_S	$10N_0 P_T/2$
Height of BS	3 m
Height of blocker	1.7 m
Height of MT	1.5 m
Blocker radius	0.4 m
BS antenna array	32×32
Number RIS elements, $M \times N$	1024 el
Environment	UMi Street Canyon [47]
Number of evaluation points, L	30
Number of repetition times, rep	1000

5.2. Lower bound analysis

In this subsection, we provide the CRLB estimation of localization error and feasibility study for cellular, D2D, and RIS-based positioning for different noise models. Delving into the details of the analysis of the maximum achievable performance of cellular, D2D, and RIS-aided positioning, we present Table 6 reporting main metrics while varying the distribution of D2D nodes when running the simulations $rep = 1000$ times per $L = 30$ points. As can be seen, when D2D relays are uniformly distributed either in $100\text{m} \times 100\text{m}$ or in the circle of radius of 20 m, the influence of outliers takes a toll on considered metrics due to the fact the geometry of the four nodes is not perfect in such cases but rather random. Regarding the performance of CRLBs under different noise models, the one with the Gaussian noise model provides lower errors due to the fact that it does not take into account distances and LoS/nLoS conditions. The results of CRLBs with the theoretical distance-dependent noise model fall between those obtained with the empirical distance-dependent noise model for 20% and 30% LoS scenarios (i.e., around 25%).

We would like to comment on the fact that in both distance-dependent noise models, RIS exhibits larger errors compared to equally placed D2D anchors owing to greater propagation loss (as also can be seen in Fig. 1). Moreover, it is worth noting all CRLBs utilizing the empirical distance-dependent noise model yield absolutely matching results when D2D relays are uniformly distributed in the circle of radius of 20 m. This can be explained by the short communication distances, which consistently provide LoS conditions.

Furthermore, we highlight that the theoretical model adeptly accounts for LoS/nLoS based on the distance-dependent LoS probabilities. For instance, for cellular, RIS, and D2D equal placement, the communication radius is around 100 m, and a closer examination of Fig. 4 reveals that the 100 m point precisely falls between the empirical distance-dependent noise models for 20% and 30% of guaranteed LoS. Hence, this observation leads us to confidently conclude that the theoretical model provides a reliable approximation.

Fig. 6 represents the localization error uncertainty for different technologies and benchmarks while running the simulation once per point, which does not collect outliers. The x and y axes represent the 2D space in which the localization is performed. The contour lines on the plots represent different levels of localization error. Each contour line connects points with the same error value. The closer the contour lines are to each other, the steeper the change in error between them. We highlight that despite symmetric anchor placement for cellular, D2D, and RIS configurations, the heteroscedastic type of noise (i.e., not cross-correlated uncertainties) leads to an asymmetric distribution of errors, as illustrated in Fig. 6. This observation aligns with the conclusions in [56]. In the case of homoscedastic noise variances, the distribution of errors would be symmetric.

Summarizing the results on minimal theoretical estimation of uncertainties, this analysis illuminates the intricate relationships between technologies, noise models, anchor distribution, and performance metrics. Moreover, the random distribution of the anchors introduces more uncertainty, leading to the presence of outliers affecting the final metrics of interest. As we navigate the complexities of positioning systems, it becomes increasingly evident that all these factors collectively shape the accuracy and reliability of localization outcomes.

5.3. Equal placement of RISs and relays

The results presented in Fig. 8(a) and Table 7(a) correspond to the first evaluation campaign. In this scenario, RISs and relay devices share the same physical positions (i.e., equidistant from the point with unknown coordinates). Note that the total power constraint is constantly employed in the relay system.

Our analysis reveals that, in this case, no single technology emerges as definitively superior across all evaluated metrics. As shown in Table 7(a), the configuration that optimizes one metric does not necessarily yield the best results for the others (see the scenarios discussed in Sections 5.4, 5.5, and 5.6). Although the uniform distribution of the devices and RIS elements leads to similar channel quality across configurations, the independent nature of the noise in these systems results in different positioning errors for each technology. Nevertheless, in this scenario, the combination of all free technologies (see “Cellular+D2D HD+RIS”) offers the lowest MSE, RMSE, 75th, and 95th percentile of the positioning errors, and standard deviation. Hence, the results confirm our hypothesis that peer cooperation can improve accuracy.

We note that high localization errors occur when there is a lot of uncertainty in the system due to various factors, one of which is noise. This noise is like random variations or disturbances that affect the RSS we estimate. We recall that, in our simulations, the noise w is modeled as a zero-mean Gaussian random variable with a standard deviation. When we calculate the measured and estimated power in a localization system, the noise can cause the estimates to vary from one instance to another, as illustrated in Fig. 7. These variations in noise can make it challenging for the system to accurately estimate the true location, leading to errors in localization.

5.4. Random placement of relays

To further evaluate the impact of D2D on localization, we randomly distribute four D2D relays within the considered area of interest, as shown in Fig. 5 (labeled as “random D2D”). All other parameters remain unchanged. As evident in Fig. 8(b) and Table 7(b), D2D localization achieves superior accuracy compared to the cellular and RIS-based methods. This can be attributed to the generally shorter distances between the anchor nodes and target node in the D2D scenario. It is important to note that the positioning accuracy can exhibit some variation, depending on the system noise characteristics (i.e., a normal distribution with $\sigma_{SF}^2 = 4$, which is independent for all the technologies). This variability is evident in the performance comparison between RIS and the cellular positioning, as illustrated in Figs. 8(a) and 8(b).

Moreover, in Fig. 8(b) and Table 7(b), RIS provides smaller errors than cellular-based positioning for most of the metrics, including the mean, standard deviation, MSE, RMSE, 75th, and 95th percentile. A significant improvement of the positioning error is provided by the combination of all three technologies with FD relaying, with a reduction of 24.9% in terms of mean error with respect to cellular positioning.

Table 6
Cramer-Rao lower bound, [m]. Results are shown in descending order of 95th PRC error.

(a) Gaussian noise									
Configuration	Min	Max	Mean	Median	Std	75th PRC	95th PRC	MSE	RMSE
D2D uniform in 100 m×100 m	1.01	332.36	3.87	2.39	6.62	3.79	10.80	58.77	7.66
D2D in circle with radius 20 m	1.01	588.23	2.19	1.63	4.14	2.19	4.57	21.95	4.68
RIS	1.30	5.28	1.72	1.52	0.44	1.94	2.67	3.16	1.78
D2D equal placement	1.30	5.28	1.72	1.52	0.44	1.94	2.67	3.16	1.78
Cellular	1.29	2.97	1.59	1.48	0.26	1.74	2.13	2.59	1.61
(b) Distance-dependent noise (Theoretical)									
Configuration	Min	Max	Mean	Median	Std	75th PRC	95th PRC	MSE	RMSE
D2D uniform in 100 m×100 m	0	947.99	11.98	7.17	21.51	11.89	34.38	606.30	24.62
D2D in circle with radius 20 m	2.55	1491.2	5.54	4.13	10.50	5.54	11.60	141.04	11.88
RIS	2.78	23.38	6.45	5.73	1.82	7.40	10.31	44.97	6.71
D2D equal placement	0	18.08	5.69	5.07	1.69	6.58	9.22	35.26	5.94
Cellular	0	14.87	4.79	4.55	0.96	5.43	6.55	23.81	4.88
(c) Distance-dependent noise (Empirical, guaranteed 10% LoS)									
Configuration	Min	Max	Mean	Median	Std	75th PRC	95th PRC	MSE	RMSE
D2D uniform in 100 m×100 m	0	892.29	10.81	6.55	19.08	10.68	30.69	480.96	21.93
D2D in circle with radius 20 m	2.52	1473.6	5.48	4.09	10.38	5.48	11.46	137.72	11.74
RIS	2.75	21.43	5.84	5.18	1.57	6.64	9.21	36.60	6.05
D2D equal placement	0	15.61	5.00	4.44	1.40	5.72	7.97	26.96	5.19
Cellular	0	9.16	3.98	3.76	0.75	4.47	5.41	16.38	4.05
(d) Distance-dependent noise (Empirical, guaranteed 20% LoS)									
Configuration	Min	Max	Mean	Median	Std	75th PRC	95th PRC	MSE	RMSE
D2D uniform in 100 m×100 m	0	892.29	10.84	6.55	19.14	10.69	30.91	483.76	21.99
D2D in circle with radius 20 m	2.52	1473.6	5.48	4.09	10.38	5.48	11.46	137.72	11.74
RIS	2.77	21.69	5.88	5.19	1.61	6.66	9.34	37.15	6.09
D2D equal placement	0	15.66	5.03	4.45	1.44	5.74	8.07	27.39	5.23
Cellular	0	10.18	4.10	3.79	0.84	4.55	5.87	17.49	4.18
(e) Distance-dependent noise (Empirical, guaranteed 30% LoS)									
Configuration	Min	Max	Mean	Median	Std	75th PRC	95th PRC	MSE	RMSE
D2D uniform in 100 m×100 m	0	892.29	11.53	6.67	21.35	11.26	33.64	588.98	24.27
D2D in circle with radius 20 m	2.52	1473.6	5.48	4.09	10.38	5.48	11.46	137.72	11.74
RIS	2.89	31.60	7.07	5.40	3.04	8.89	13.55	59.27	7.70
D2D equal placement	0	26.06	6.11	4.62	2.72	7.74	11.95	44.75	6.69
Cellular	0	22.24	5.59	4.91	2.02	6.89	9.70	35.36	5.95
(f) Distance-dependent noise (Empirical, guaranteed 70% LoS)									
Configuration	Min	Max	Mean	Median	Std	75th PRC	95th PRC	MSE	RMSE
D2D uniform in 100 m×100 m	0	1320.9	17.72	9.96	34.09	17.99	52.87	1476.6	38.43
D2D in circle with radius 20 m	2.52	1473.6	5.48	4.09	10.38	5.48	11.46	137.72	11.74
RIS	2.90	32.63	10.13	9.50	3.16	11.88	16.30	112.73	10.62
D2D equal placement	0	27.30	8.99	8.46	2.90	10.62	14.59	89.28	9.45
Cellular	0	24.05	8.24	8.20	1.84	9.49	11.11	71.23	8.44

5.5. Random placement of relays within 20 m radius

The next step is to analyze the performance when the D2D relays are randomly distributed within a maximum distance of 20 m around the device. The results reported in Fig. 8(c) and Table 7(c) demonstrate that a substantial improvement in D2D localization positioning accuracy is achieved. In this case, the positions of BSs and RISs are fixed, and the D2D devices are located much closer to the node with an unknown location (see visualization on the right part of Fig. 5).

In contrast to the two previous scenarios, the D2D localization (with and without FD) now has the lowest mean positioning error, being even better than the combination of all technologies. This also happens for the other metrics except the median, where cellular provides the best results. In this case, D2D localization is much better than cellular and RIS, rendering the integration of all three technologies ineffective. The positioning errors individually provided with each technology cannot be compensated by each other. The difference between the two D2D schemes (i.e., half-duplex (HD) and FD) is minor in this case because the distance between MTs is shorter.

5.6. nLoS : Random placement of relays

As the final use case, we analyze the positioning precision using different technologies in the UMi Street Canyon nLoS scenario. We consider, a path loss exponent (PLE) with $\zeta = 3.19$ and $\sigma_{SF}^2 = 7.82$. The results are reported in Fig. 8(d) and Table 7(d). The design of RIS is special as it provides a virtual LoS path when a direct BS-UE path is blocked [55]. Thus, all RISs are always in LoS. Given the presence of obstacles in the paths, the performance is worse than in the LoS scenario presented in Fig. 8(b). In this case, the combination of all technologies provides the best results, as the estimated positions are distributed around the real location, and the errors can be balanced.

Additionally, for this use case, we have computed the centroid of the three position estimates with the median instead of the average when combining the three technologies. This approach with the median can only be applied when the number of technologies combined is 3 or higher. This proposed approach in this use case has reduced the mean localization error by 41.36% compared to the traditional centroid calculation with the mean. It is worth highlighting that the median may be a better approach to fuse data because it is more robust to outliers. In this case, the cellular positioning is completely failing, and the other two provide similar accuracy. The mean sensor fusion is penalized by

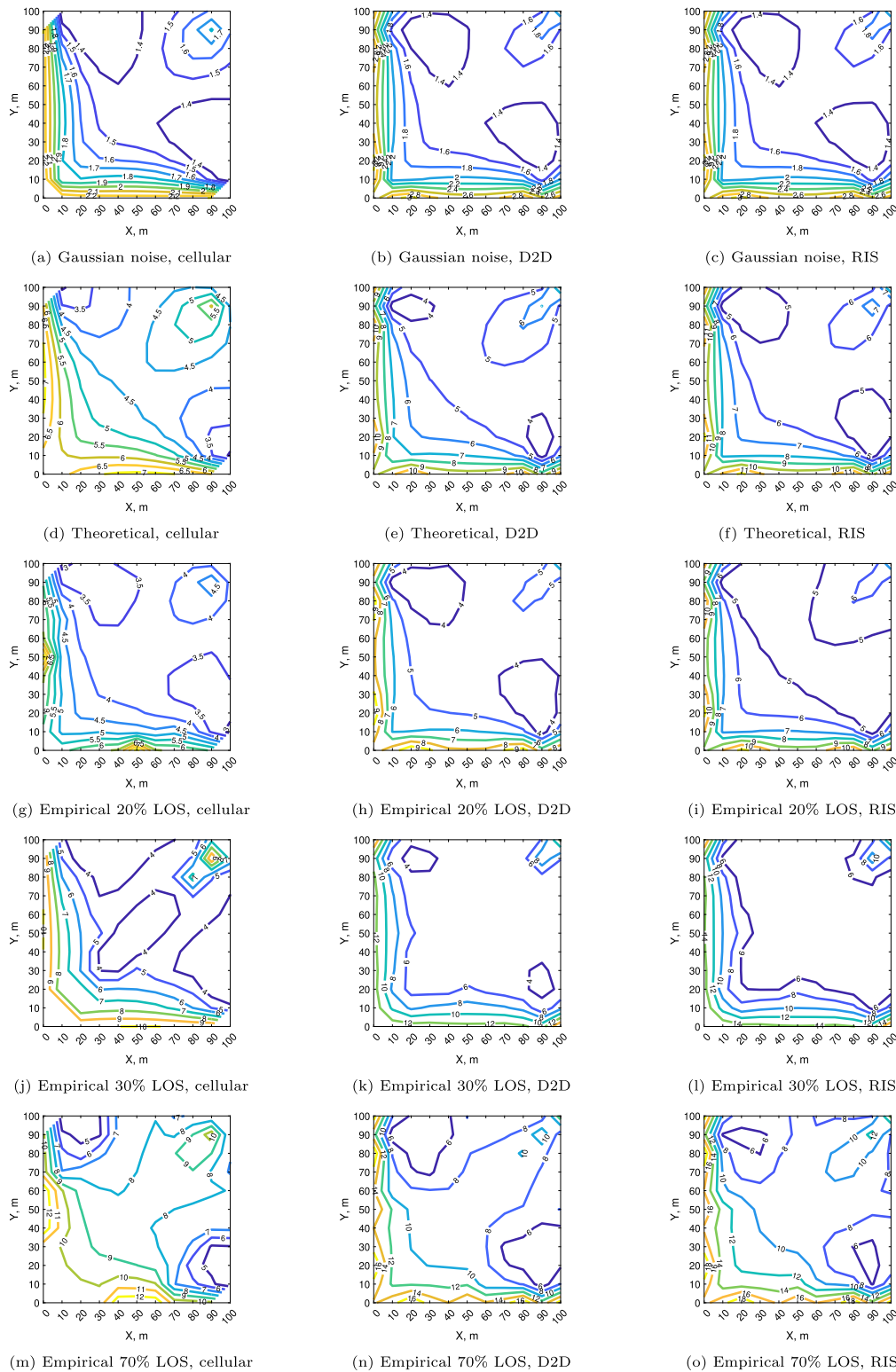


Fig. 6. Theoretical lower bounds, equal placement of RISs and relays.

the wrong estimate from the cellular positioning, while the median sensor fusion ignores it and provides a better overall localization.

5.7. Summary and general discussion of results

The analysis of the results of the four scenarios brings us some relevant discussion. When D2D or RIS provides significantly better results

than the other approaches, the combination of multiple technologies may not work. That is, if a technology is providing significantly worse results than the winning one, we should not consider it for the sensor fusion (see Fig. 8(c) and Table 7(c)). Only when these three technologies (i.e., cellular, D2D and RIS) provide similar overall results, their combination outperforms any of the individual solutions.

Table 7
Individual errors, [m]. Results are shown in descending order of 95th PRC error.

(a) LoS, PLE=2.1, SF=4. RISs and relays have the same locations									
Configuration	MIN	MAX	MEAN	MEDIAN	STD	75 th PRC	95 th PRC	MSE	RMSE
Cellular	0.0176	1024.0	34.68	5.80	55.56	52.73	148.69	4290.3	65.50
RIS	0.020	756.46	34.94	10.36	51.93	49.33	140.35	3917.4	62.58
D2D HD	0.0124	895.01	28.97	7.27	44.78	40.90	122.29	2844.2	53.33
D2D FD	0.0072	597.89	28.98	7.30	44.50	41.24	121.79	2820.6	53.10
Cellular+RIS	0.011	512.31	32.80	18.83	37.88	50.07	107.70	2510.7	50.10
Cellular+D2D FD	0.020	511.73	29.89	15.57	35.58	46.00	101.35	2159.0	46.46
Cellular+D2D HD	0.039	553.51	29.85	15.56	35.49	46.18	100.86	2151.0	46.37
Cellular+D2D FD+RIS	0.018	341.37	29.91	22.18	29.68	44.08	88.93	1775.8	42.14
Cellular+D2D HD+RIS	0.026	369.23	29.87	22.19	29.63	44.01	88.76	1770.1	42.07
(b) LoS, PLE=2.1, SF=4. D2D relays are uniformly distributed within 100m×100m									
Configuration	MIN	MAX	MEAN	MEDIAN	STD	75 th PRC	95 th PRC	MSE	RMSE
Cellular	0.012	633.62	34.65	5.85	55.55	52.26	150.23	4286.1	65.47
RIS	0.039	730.56	34.29	10.39	51.44	47.79	137.38	3821.1	61.82
Cellular+RIS	0.010	401.76	32.47	18.04	37.58	49.38	106.38	2466.2	49.66
D2D HD	0.032	444.76	29.47	18.70	33.54	38.44	95.46	1993.4	44.65
D2D FD	0.018	582.55	29.21	18.45	33.86	37.86	94.65	1999.7	44.72
Cellular+D2D HD	0.035	319.29	26.93	16.41	29.12	38.03	85.99	1573.3	39.66
Cellular+D2D FD	0.054	328.85	26.77	16.08	29.09	38.19	84.65	1563.0	39.53
Cellular+D2D HD+RIS	0.041	270.54	26.18	18.47	25.28	37.24	76.11	1324.6	36.40
Cellular+D2D FD+RIS	0.035	264.09	26.02	18.36	25.18	37.14	75.20	1310.6	36.20
(c) LoS, PLE=2.1, SF=4. D2D relays are uniformly distributed within circle with radius of 20m									
Configuration	MIN	MAX	MEAN	MEDIAN	STD	75 th PRC	95 th PRC	MSE	RMSE
Cellular	0.027	959.19	34.74	5.88	55.92	52.55	149.77	4333.6	65.83
RIS	0.0159	666.71	34.34	10.43	51.12	47.85	138.66	3792.6	61.58
Cellular+RIS	0.039	487.98	32.52	18.36	37.65	49.74	106.23	2475.3	49.75
Cellular+D2D FD	0.0255	477.32	21.77	11.66	27.09	30.30	76.12	1207.3	34.75
Cellular+D2D HD	0.0327	466.58	21.81	11.86	27.04	30.29	75.81	1207.1	34.74
Cellular+D2D FD+RIS	0.0123	327.66	23.39	15.42	24.41	33.69	71.59	1142.9	33.81
Cellular+D2D HD+RIS	0.0223	325.10	23.40	15.40	24.41	33.80	71.31	1143.4	33.81
D2D HD	0.00017	340.85	16.10	7.38	19.61	25.07	54.83	643.84	25.37
D2D FD	0.000025	250.32	15.91	7.15	19.35	24.80	54.57	627.47	25.05
(d) NLoS, PLE=3.19, SF=7.82. D2D relays are uniformly distributed within 100m×100m square									
Configuration	MIN	MAX	MEAN	MEDIAN	STD	75 th PRC	95 th PRC	MSE	RMSE
Cellular	0.0174	1056.4	47.52	6.85	80.25	70.66	200.65	8698.8	93.27
RIS	0.0074	571.01	34.75	10.35	51.03	49.03	140.99	3811.7	61.74
Cellular+RIS	0.0091	598.68	39.11	22.75	47.19	58.42	129.59	3756.8	61.29
D2D HD	0.0225	1472.6	35.96	21.28	47.45	44.62	120.34	3545.0	59.54
D2D FD	0.0236	1095.6	35.77	21.24	46.90	44.34	118.14	3478.9	58.98
Cellular+D2D HD	0.0415	736.62	36.00	20.79	43.14	49.62	116.45	3156.5	56.18
Cellular+D2D FD	0.1104	550.16	35.87	20.29	43.10	48.96	116.42	3145.2	56.08
Cellular+D2D FD+RIS	0.0653	413.50	32.18	22.17	33.04	45.01	95.71	2127.0	46.12
Cellular+D2D HD+RIS	0.0204	504.34	32.29	22.18	33.07	45.56	94.69	2136.5	46.22
Cellular+D2D HD+RIS*	0.0135	357.33	18.97	6.80	28.97	20.95	81.08	1198.7	34.62
Cellular+D2D FD+RIS*	0.0135	357.33	18.87	6.79	28.82	20.83	80.63	1186.8	34.45

* this configuration uses median for position-level sensor fusion among the three technologies

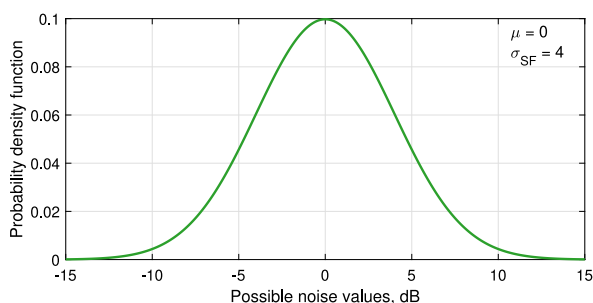


Fig. 7. Visualization of Gaussian noise probability density function.

The noise is the main source of positioning error, as already identified in the literature. The results presented in this work are based on the combination of D2D, RIS, and cellular data with independent and uncorrelated sources of noise, being the combination of those

three positioning sources optimal as the error sources due to noise are compensating each other. First, this finding is confirmed by [56], stating that in the case of uncorrelated noise, the number of anchors is inversely proportional to the estimation uncertainty. Furthermore, we base our assumption of uncorrelated noise on the fact that if each measurement is taken independently from the others, the noise (e.g., when constructing CRLB) can be considered non-correlated in the case of TOA system, which is the most widespread for RSS measurements and is the case of this work. Differently, if more than one measurement is used for obtaining a system equation (TDOA system), then the measurements and the noise are correlated. Moreover, spatial channels and objects that contribute to the fading introducing noise in the system are different for each technology. For example, in the case of long-range cellular technology, the objects can be buildings and other large-scale objects, while in the case of short-range D2D communications, the objects are rather humans, trees, etc. Anyway, we should bear in mind that the anchors' location impacts the positioning performance. In particular, the lowest errors occur when the D2D relays are located close to the MT with unknown coordinates, as shown in Fig. 8(c) and Table 7(c).

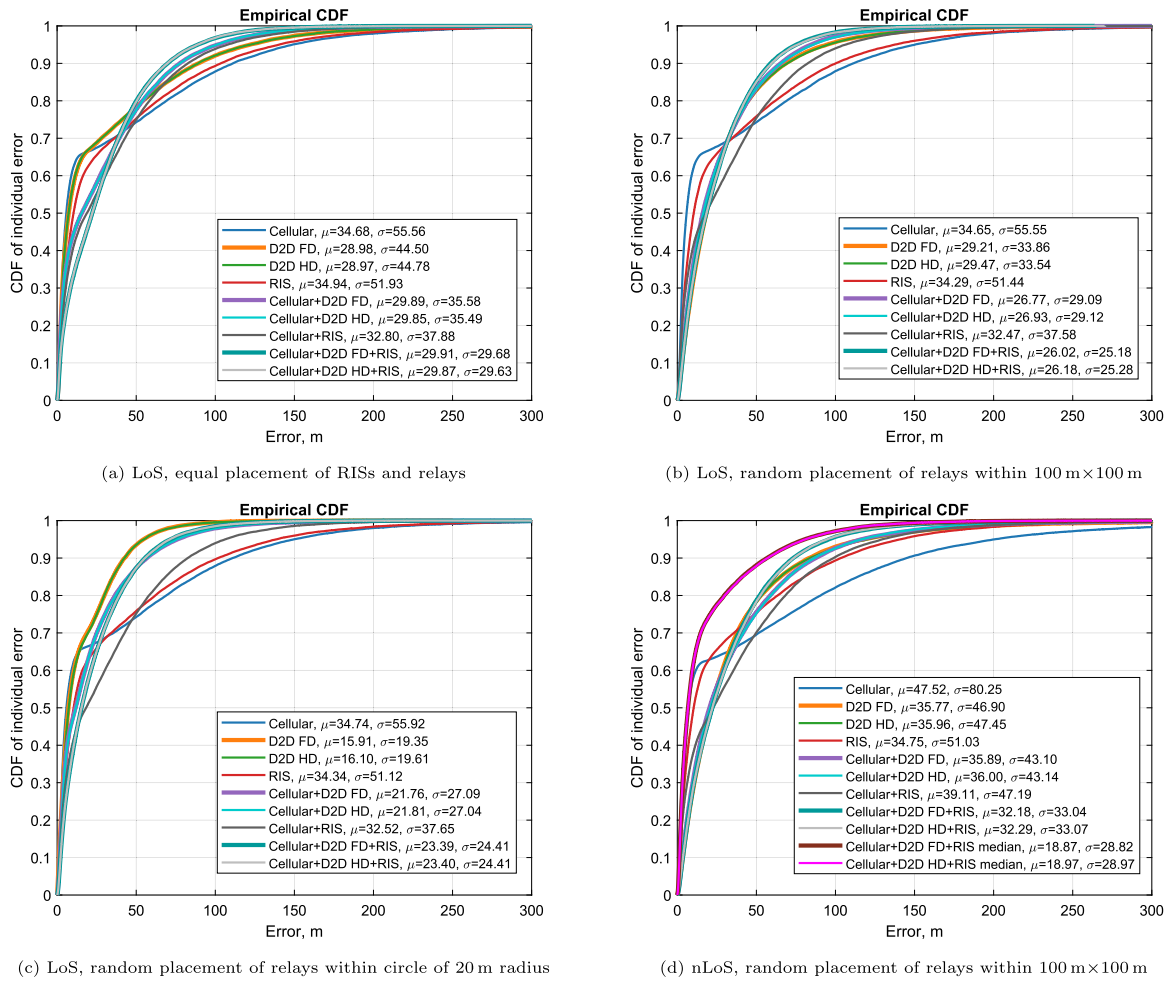


Fig. 8. CDF of individual error.

The selection of the four use cases covers different scenarios and provides more general results for the proposed method as follows.

- cellular localization is significantly enhanced when RIS is applied only for the nLoS case, being the improvement minor in the LoS case;
- in D2D, the location of devices defines the positioning accuracy in both LoS and nLoS scenarios;
- sensor fusion especially improves the positioning error in terms of the median.

6. Conclusions and future work

In this study, we presented a theoretical (probabilistic) distance-dependent noise model in the CRLB variance range estimation, which also accounts for nLoS for D2D- and RIS-aided, and cellular positioning systems. Then, we compared them in terms of positioning precision (i.e., both lower bounds and positioning error). Through our simulation campaign, we identified the scenarios where one technology outperforms the other, as well as presented the localization performance of the D2D-, RIS-assisted cellular localization. In addition, we discussed the role of mean and median metrics in localization systems.

Based on the findings of this study, we draw the following conclusions. First, RIS-aided localization is a viable option when the distribution of D2D anchors is limited and/or when D2D/cellular path is blocked. Alternately, relaying is more effective than RIS positioning due to the short distances. Moreover, we emphasize that when the improvement of RIS and D2D over cellular positioning is marginal

(i.e., less than 50%), using a combination of RIS, D2D, and cellular technologies results in the lowest positioning errors. Further, when one of the technologies shows a significant improvement over cellular positioning, it offers the best performance among all configurations. Moreover, using the median for position-level sensor fusion in cases where the locations are obtained from the three methods can reduce the positioning error by 41% compared to mean fusion, and this approach can be considered practical for minimizing the mean error.

As future works, we highlight the following directions:

- Although the proposed distance-dependent noise model that we use for CRLB is general and applicable to various scenarios, it still relies on LoS probability that needs to be recalculated for different environments defined in 3GPP. While the approach is theoretically applicable across a wide range of scenarios and it utilizes 3GPP compliant models that are designed based on empirical measurements and ray tracing results, further adjustments and validations of the distance-dependent noise model might be needed in practical applications.
- As discussed above, the location and geometry of the anchors impact the accuracy of positioning. However, since the device coordinates are unknown, this poses a challenge. To deal with it, optimization of the location of the infrastructure should be performed based on metaheuristics and optimization algorithms [62, 63].

Reproducible Research: The open-source code is available from <https://github.com/NadezhdaChukhno/Cooperative-RSSI-based-Localizat>

ion-using-cellular-data-D2D-and-RIS. The final release is also published in Zenodo to guarantee long-term access to the developed source code: <https://doi.org/10.5281/zenodo.15271732>.

CRedit authorship contribution statement

Nadezhda Chukhno: Writing – review & editing, Writing – original draft, Visualization, Validation, Methodology, Investigation, Formal analysis, Data curation, Conceptualization. **Tomas Bravenec:** Writing – review & editing, Visualization, Validation, Methodology, Investigation, Formal analysis, Data curation. **Javier Díez-González:** Methodology. **Sergio Trilles:** Writing – review & editing, Writing – original draft, Supervision, Methodology, Conceptualization. **Joaquín Torres-Sospedra:** Writing – review & editing, Writing – original draft, Supervision, Investigation, Conceptualization. **Antonio Iera:** Writing – review & editing, Supervision, Conceptualization. **Giuseppe Araniti:** Supervision, Conceptualization.

Declaration of competing interest

The authors declare that they have no known competing financial interests or personal relationships that could have appeared to influence the work reported in this paper.

Acknowledgments

The authors gratefully acknowledge funding from European Union's Horizon 2020 Research and Innovation programme under the Marie Skłodowska Curie grant agreements No. 813278 (A-WEAR: A network for dynamic wearable applications with privacy constraints, <http://www.a-wear.eu/>) and No. 101023072 (ORIENTATE: Low-cost Reliable Indoor Positioning in Smart Factories, <http://orientate.dsi.uminho.pt>); Sergio Trilles has been funded by the Juan de la Cierva - Incorporación postdoctoral programme of the Ministerio de Ciencia e Innovación - Spanish government (IJC2018-035017-I) funded by MCIN/AEI/10.13039/501100011033 and by “ERDF, a way of making Europe”, by the European Union. J. Torres-Sospedra acknowledges funding from Generalitat Valenciana, Spain (CIDEXG/2023/17, Conselleria d'Educació, Universitats i Ocupació).

Data availability

The link to data/code has been shared.

References

- [1] C. De Lima, D. Belot, R. Berkvens, A. Bourdoux, D. Dardari, M. Guillaud, M. Isomursu, E.-S. Lohan, Y. Miao, A.N. Barreto, et al., Convergent communication, sensing and localization in 6G systems: An overview of technologies, opportunities and challenges, *IEEE Access* 9 (2021) 26902–26925.
- [2] M. Tao, H. Jun, Z. Jiahao, L. Wengang, Location-driven beamforming for massive multi-user MIMO systems, *J. Syst. Eng. Electron.* (2024).
- [3] T. Kallehauge, M.V. Vejling, P. Ramírez-Espinosa, K. Kansanen, H. Wymeersch, P. Popovski, On the statistical relation of ultra-reliable wireless and location estimation, *IEEE Trans. Wirel. Commun.* (2024).
- [4] D.K.P. Tan, J. He, Y. Li, A. Bayesteh, Y. Chen, P. Zhu, W. Tong, Integrated sensing and communication in 6G: Motivations, use cases, requirements, challenges and future directions, in: 2021 1st IEEE International Online Symposium on Joint Communications & Sensing, JC&S, IEEE, 2021.
- [5] Z. Xiao, Y. Zeng, An overview on integrated localization and communication towards 6G, *Sci. China Inf. Sci.* 65 (3) (2022) 1–46.
- [6] H. Wymeersch, D. Shrestha, C.M. De Lima, V. Yajnanarayana, B. Richerzhagen, M.F. Keskin, K. Schindhelm, A. Ramirez, A. Wolfgang, M.F. De Guzman, et al., Integration of communication and sensing in 6G: A joint industrial and academic perspective, in: 2021 IEEE 32nd Annual International Symposium on Personal, Indoor and Mobile Radio Communications, PIMRC, IEEE, 2021.
- [7] P. Zhang, J. Lu, Y. Wang, Q. Wang, Cooperative localization in 5G networks: A survey, *Ict Express* 3 (1) (2017) 27–32.

- [8] M. Gerasimenko, D. Moltchanov, M. Gapeyenko, S. Andreev, Y. Koucheryavy, Capacity of multiconnectivity mmwave systems with dynamic blockage and directional antennas, *IEEE Trans. Veh. Technol.* 68 (4) (2019) 3534–3549.
- [9] H. Sarihdeen, N. Saeed, T.Y. Al-Naffouri, M.-S. Alouini, Next generation terahertz communications: A rendezvous of sensing, imaging, and localization, *IEEE Commun. Mag.* 58 (5) (2020) 69–75.
- [10] S. Series, Comparison of Time-Difference-of-Arrival and Angle-of-Arrival Methods of Signal Geolocation, ITU, Geneva, Switzerland, 2011.
- [11] Z. Zheng, L. Liu, W. Hu, Accuracy of ranging based on DMT visible light communication for indoor positioning, *IEEE Photonics Technol. Lett.* 29 (8) (2017) 679–682.
- [12] K. Järvinen, H. Leppäkoski, E.-S. Lohan, P. Richter, T. Schneider, O. Tkachenko, Z. Yang, PILOT: Practical privacy-preserving indoor localization using outsourcing, in: 2019 IEEE European Symposium on Security and Privacy, EuroS&P, IEEE, 2019, pp. 448–463.
- [13] V. Shubina, A. Ometov, S. Andreev, D. Niculescu, E.S. Lohan, Privacy versus location accuracy in opportunistic wearable networks, in: 2020 International Conference on Localization and GNSS, ICL-GNSS, IEEE, 2020.
- [14] J. Zhang, Z. Zheng, Z. Fei, Z. Han, Energy-efficient multi-user localization in the RIS-assisted IoT networks, *IEEE Internet Things J.* (2022).
- [15] N. Chukhno, S. Trilles, J. Torres-Sospedra, A. Iera, G. Araniti, D2D-based cooperative positioning paradigm for future wireless systems: A survey, *IEEE Sensors J.* (2021).
- [16] S. Khandker, J. Torres-Sospedra, T. Ristaniemi, Improving RF fingerprinting methods by means of D2D communication protocol, *Electron.* 8 (1) (2019) 97.
- [17] R.M. Buehrer, H. Wymeersch, R.M. Vaghefi, Collaborative sensor network localization: Algorithms and practical issues, *Proc. IEEE* 106 (6) (2018) 1089–1114.
- [18] M. Karlsson, F. Karlsson, Cooperative indoor positioning by exchange of bluetooth signals and state estimates between users, in: 2016 European Control Conference, ECC, IEEE, 2016, pp. 1440–1444.
- [19] D. Salami, R. Hasibi, S. Savazzi, T. Michoel, S. Sigg, Integrating sensing and communication in cellular networks via nr sidelink, 2021, arXiv preprint arXiv:2109.07253.
- [20] A. Dammann, R. Raulefs, S. Zhang, On prospects of positioning in 5G, in: 2015 IEEE International Conference on Communication Workshop, ICCW, IEEE, 2015, pp. 1207–1213.
- [21] Y. Lu, M. Koivisto, J. Talvitie, E. Rastorgueva-Foi, T. Levanen, E.S. Lohan, M. Valkama, Joint positioning and tracking via NR sidelink in 5G-empowered industrial IoT: Releasing the potential of V2X technology, 2021, arXiv preprint arXiv:2101.06003.
- [22] M.F.I. Azam, Q. Ni, M. Dong, H.B. Pervaiz, Cooperative localization based interference avoidance in cognitive radio networks, in: ICC 2021-IEEE International Conference on Communications, IEEE, 2021.
- [23] P. Pascacio, J. Torres-Sospedra, S. Casteleyn, E.S. Lohan, A collaborative approach using neural networks for BLE-rss lateration-based indoor positioning, 2022, arXiv preprint arXiv:2205.10559.
- [24] J.-W. Qiu, C.C. Lo, C.-K. Lin, Y.-C. Tseng, A D2D relative positioning system on smart devices, in: 2014 IEEE Wireless Communications and Networking Conference, WCNC, IEEE, 2014, pp. 2168–2172.
- [25] K. Keykhosravi, M.F. Keskin, S. Dwivedi, G. Seco-Granados, H. Wymeersch, Semi-passive 3D positioning of multiple RIS-enabled users, *IEEE Trans. Veh. Technol.* 70 (10) (2021) 11073–11077.
- [26] C. Pan, H. Ren, K. Wang, J.F. Kolb, M. El-kashlan, M. Chen, M. Di Renzo, Y. Hao, J. Wang, A.L. Swindlehurst, et al., Reconfigurable intelligent surfaces for 6G systems: Principles, applications, and research directions, *IEEE Commun. Mag.* 59 (6) (2021) 14–20.
- [27] M. Di Renzo, K. Ntontin, J. Song, F.H. Danufane, X. Qian, F. Lazarakis, J. De Rosny, D.-T. Phan-Huy, O. Simeone, R. Zhang, et al., Reconfigurable intelligent surfaces vs. Relaying: Differences, similarities, and performance comparison, *IEEE Open J. Commun. Soc.* 1 (2020) 798–807.
- [28] E. Björnson, Ö. Özdogan, E.G. Larsson, Reconfigurable intelligent surfaces: Three myths and two critical questions, *IEEE Commun. Mag.* 58 (12) (2020) 90–96.
- [29] Q. Wu, S. Zhang, B. Zheng, C. You, R. Zhang, Intelligent reflecting surface aided wireless communications: A tutorial, *IEEE Trans. Commun.* (2021).
- [30] E. Björnson, Ö. Özdogan, E.G. Larsson, Intelligent reflecting surface versus decode-and-forward: How large surfaces are needed to beat relaying? *IEEE Wirel. Commun. Lett.* 9 (2) (2019) 244–248.
- [31] H. Wymeersch, J. He, B. Denis, A. Clemente, M. Juntti, Radio localization and mapping with reconfigurable intelligent surfaces: Challenges, opportunities, and research directions, *IEEE Veh. Technol. Mag.* 15 (4) (2020) 52–61.
- [32] J. He, H. Wymeersch, T. Sanguanpuak, O. Silvén, M. Juntti, Adaptive beamforming design for mmwave RIS-aided joint localization and communication, in: 2020 IEEE Wireless Communications and Networking Conference Workshops, WCNCW, IEEE, 2020.

- [33] Y. Cui, H. Yin, Channel estimation for RIS-aided mmwave communications via 3D positioning, in: 2021 IEEE/CIC International Conference on Communications in China (ICCC Workshops), IEEE, 2021, pp. 399–404.
- [34] M. Di Renzo, A. Zappone, M. Debbah, M.-S. Alouini, C. Yuen, J. De Rosny, S. Tretyakov, Smart radio environments empowered by reconfigurable intelligent surfaces: How it works, state of research, and the road ahead, *IEEE J. Sel. Areas Commun.* 38 (11) (2020) 2450–2525.
- [35] M. Heino, D. Korpi, T. Huusari, E. Antonio-Rodriguez, S. Venkatasubramanian, T. Riihonen, L. Anttila, C. Icheln, K. Haneda, R. Wichman, et al., Recent advances in antenna design and interference cancellation algorithms for in-band full duplex relays, *IEEE Commun. Mag.* 53 (5) (2015) 91–101.
- [36] A. Elzanaty, A. Guerra, F. Guidi, M.-S. Alouini, Reconfigurable intelligent surfaces for localization: Position and orientation error bounds, *IEEE Trans. Signal Process.* 69 (2021) 5386–5402.
- [37] M. Ammous, S. Valaee, Cooperative positioning with the aid of reconfigurable intelligent surfaces and device-to-device communications in mmwave, in: 2022 IEEE 33rd Annual International Symposium on Personal, Indoor and Mobile Radio Communications, PIMRC, IEEE, 2022, pp. 683–688.
- [38] M. Ammous, S. Valaee, Cooperative positioning with the aid of reconfigurable intelligent surfaces and zero access points, in: 2022 IEEE 96th Vehicular Technology Conference (VTC2022-Fall), IEEE, 2022, pp. 1–5.
- [39] M. Ammous, H. Chen, H. Wymeersch, S. Valaee, Zero access points 3D cooperative positioning via RIS and sidelink communications, 2023, arXiv preprint arXiv:2305.08287.
- [40] Z. Lu, Y. Zhao, Y. Ge, C.-Z. Xu, RACLN: Reconfigurable intelligent surface as anchors for cooperative localization of wireless sensor network, *IEEE Internet Things J.* (2024).
- [41] N. Alam, A.G. Dempster, Cooperative positioning for vehicular networks: Facts and future, *IEEE Trans. Intell. Transp. Syst.* 14 (4) (2013) 1708–1717.
- [42] T. Bravenec, M. Gould, T. Fryza, J. Torres-Sospedra, Influence of measured radio map interpolation on indoor positioning algorithms, *IEEE Sensors J.* (2023).
- [43] M.K. Simon, M.-S. Alouini, Digital communications over fading channels (MK Simon and MS Alouini; 2005), *IEEE Trans. Inform. Theory* 54 (7) (2008) 3369–3370.
- [44] K. Pahlavan, A.H. Levesque, *Wireless Information Networks*, John Wiley & Sons, 2005.
- [45] S. Mazuelas, F.A. Lago, D. González, A. Bahillo, J. Blas, P. Fernandez, R.M. Lorenzo, E.J. Abril, Dynamic estimation of optimum path loss model in a RSS positioning system, in: 2008 IEEE/ION Position, Location and Navigation Symposium, IEEE, 2008, pp. 679–684.
- [46] J. Du, C. Yuan, M. Yue, T. Ma, A novel localization algorithm based on RSSI and multilateration for indoor environments, *Electron.* 11 (2) (2022) 289.
- [47] 3GPP, Study on Channel Model for Frequencies from 0.5 to 100 GHz (Release 14), 3GPP TR 38.901 V14.1.1, 2017.
- [48] N. Docomo, 5G Channel Model for Bands up to 100 GHz, Tech. Rep., Tech. Report, Oct, 2016.
- [49] M. Peter, K. Haneda, S. Nguyen, A. Karttunen, J. Järveläinen, Measurement results and final mmwave channel models, *Deliv. D2 2* (2017).
- [50] M. Gapeyenko, V. Petrov, D. Moltchanov, M.R. Akdeniz, S. Andreev, N. Himayat, Y. Koucheryavy, On the degree of multi-connectivity in 5G millimeter-wave cellular urban deployments, *IEEE Trans. Veh. Technol.* 68 (2) (2018) 1973–1978.
- [51] G.R. MacCartney, T.S. Rappaport, S. Rangan, Rapid fading due to human blockage in pedestrian crowds at 5g millimeter-wave frequencies, in: GLOBECOM 2017-2017 IEEE Global Communications Conference, IEEE, 2017, pp. 1–7.
- [52] M. Gapeyenko, A. Samuylov, M. Gerasimenko, D. Moltchanov, S. Singh, E. Aryafar, S.-p. Yeh, N. Himayat, S. Andreev, Y. Koucheryavy, Analysis of human-body blockage in urban millimeter-wave cellular communications, in: 2016 IEEE International Conference on Communications, ICC, IEEE, 2016.
- [53] S. Zeng, H. Zhang, B. Di, Z. Han, L. Song, Reconfigurable intelligent surface (RIS) assisted wireless coverage extension: RIS orientation and location optimization, *IEEE Commun. Lett.* 25 (1) (2020) 269–273.
- [54] S.W. Ellingson, Path loss in reconfigurable intelligent surface-enabled channels, in: 2021 IEEE 32nd Annual International Symposium on Personal, Indoor and Mobile Radio Communications, PIMRC, IEEE, 2021, pp. 829–835.
- [55] I. Yildirim, A. Uyrus, E. Basar, Modeling and analysis of reconfigurable intelligent surfaces for indoor and outdoor applications in future wireless networks, *IEEE Trans. Commun.* 69 (2) (2020) 1290–1301.
- [56] D. Fontanelli, F. Shamsfakhr, L. Palopoli, Cramer-rao lower bound attainment in range-only positioning using geometry: The G-WLS, *IEEE Trans. Instrum. Meas.* 70 (2021) 1–14.
- [57] S.M. Kay, *Fundamentals of Statistical Signal Processing: Estimation Theory*, Prentice-Hall, Inc., 1993.
- [58] R. Álvarez, J. Díez-González, E. Alonso, L. Fernández-Robles, M. Castejón-Limas, H. Perez, Accuracy analysis in sensor networks for asynchronous positioning methods, *Sensors* 19 (13) (2019) 3024.
- [59] ISO Central Secretary, Information Technology—Real Time Locating Systems—Test and Evaluation of Localization and Tracking Systems, Standard ISO/IEC JTC 1/SC 31, International Organization for Standardization, 2016, URL <https://www.iso.org/standard/62090.html>.
- [60] F. Potorti, A. Crivello, F. Palumbo, The EvAAL evaluation framework and the IPIN competitions, in: *Geographical and Fingerprinting Data To Create Systems for Indoor Positioning and Indoor/Outdoor Navigation*, Elsevier, 2019, pp. 209–224.
- [61] D. Solomitckii, A. Orsino, S. Andreev, Y. Koucheryavy, M. Valkama, Characterization of mmwave channel properties at 28 and 60 GHz in factory automation deployments, in: 2018 IEEE Wireless Communications and Networking Conference, WCNC, IEEE, 2018.
- [62] R. Alvarez, J. Díez-Gonzalez, N. Strisciuglio, H. Perez, Multi-objective optimization for asynchronous positioning systems based on a complete characterization of ranging errors in 3D complex environments, *IEEE Access* 8 (2020) 43046–43056.
- [63] W. Zhao, A. Goudar, A.P. Schoellig, Finding the right place: Sensor placement for UWB time difference of arrival localization in cluttered indoor environments, *IEEE Robot. Autom. Lett.* 7 (3) (2022) 6075–6082.



Nadezhda Chukhno received Graduation from RUDN University, Russia, the B.Sc. degree in business informatics in 2017, the M.Sc. degree in fundamental informatics and information technologies in 2019, and the Double Ph.D. degree in information engineering with the H2020 MCSA ITN/EJD A-WEAR Project, Mediterranean University of Reggio Calabria, Italy and Jaume I University, Spain, in 2023. She is a Postdoctoral Researcher with Tampere University, Finland. Her research interests include wireless communications, 5G+ networks, and ML.



Tomas Bravenec received double doctoral degree from University Jaume I Spain and Brno University of Technology, Czechia. Previously he received his masters and bachelors degree in electronics and communications from Brno University of Technology, Czechia in 2019 and 2017 respectively. His research interests include machine learning, indoor localization, and privacy and security issues related to wearable applications.



Javier Díez-González was born in León, Spain, in 1994. He received the B.S. degree in aerospace engineering, the M.S. degree in aeronautical engineering, and the Ph.D. degree from the University of León, in 2016, 2018, and 2020, respectively, and the M.S. degree in artificial intelligence from the International University of Valencia, in 2021. He has also followed the leadership program of the University Francisco de Vitoria, Madrid, where he graduated, in 2017. He is currently a Researcher with the Department of Mechanical, Computer, and Aerospace Engineering, University of León, where he is also a Lecturer in mechanics. His research interests include high-performance localization, artificial intelligence, and industry 4.0.



Sergio Trilles has a PhD in Integration of Geospatial Information from Jaume I University in 2015, and he is currently a post-doctoral fellow at University Jaime I, holding a Juan de la Cierva - Incorporación fellowship. His research lines are centered on geospatial fields such as the Internet of Things (sensors), interoperability, geoprocessing, or web mapping. He is the author of more than ninety journal and conference peer-reviewed publications.



Joaquín Torres-Sospedra is Senior Researcher at Departament d'Informàtica, Universitat de València. He has authored more than 190 articles in journals and conference proceedings. His current research interests include indoor positioning solutions based on Wi-Fi & BLE, Machine Learning and Evaluation. He is the chair of the Smartphone-based track of IPIN Competition and the IPIN International Standards Committee.



Antonio Iera graduated in computer engineering from the University of Calabria in 1991, and received a Master's degree in IT from CEFRIEL/Politecnico di Milano in 1992 and a Ph.D. degree from the University of Calabria in 1996. From 1997 to 2019 he has been with the University Mediterranea, Italy, and currently holds the position of full professor of Telecommunications at the University of Calabria, Italy. His research interests include next-generation mobile, wireless systems, and the Internet of Things.



Giuseppe Araniti received the Laurea degree and the Ph.D. degree in electronic engineering from the University Mediterranea of Reggio Calabria, Italy, in 2000 and 2004, respectively. He is currently an Associate Professor of telecommunications with the University Mediterranea of Reggio Calabria. His major area of research is on 5G/6G networks, including personal communications, enhanced wireless and satellite systems, traffic and radio resource management, multicast and broadcast services, device-to-device (D2D), and machine-type communications (M2M/MTC).